Solar Energy Materials & Solar Cells 272 (2024) 112879

Contents lists available at ScienceDirect

Solar Energy Materials and Solar Cells

journal homepage: www.elsevier.com/locate/solmat

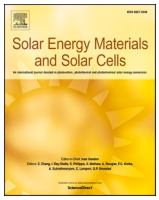

Ion-migration analysis of degradation caused by outdoor exposure and accelerated stress testing in perovskite solar cells

Takeshi Tayagaki *, Sayaka Hirooka, Haruka Kobayashi, Kohei Yamamoto, Takurou N. Murakami, Masahiro Yoshita

National Institute of Advanced Industrial Science and Technology (AIST), Tsukuba, Ibaraki 305-8568, Japan

ARTICLE INFO

Keywords:
Accelerated stress test
Degradation
Ion migration
Outdoor exposure
Perovskite solar cell

ABSTRACT

In this study, we conducted outdoor exposure testing and investigated the degradation mechanism of perovskite solar cells deployed in the field. We conducted a detailed failure analysis to identify specific degradation modes induced by outdoor exposure, using current–voltage curve measurements, maximum power evaluation, and mobile-ion analysis. This analysis revealed a significant change in the ion-migration current response of the devices after exposure. These changes suggest that the modification of mobile ions and formation of defects within the perovskite materials are likely the primary causes of degradation. Additionally, we compared the solar cell characteristics observed after the field test with the results of controlled indoor accelerated stress tests, which included exposure to visible light, ultraviolet (UV) irradiation, and thermal stress. Our findings highlight that the degradation patterns induced by UV irradiation at elevated temperatures closely resemble those caused by outdoor stress. We also discuss indoor test conditions that replicate the degradation phenomena experienced during outdoor exposure. This ability to replicate outdoor degradation phenomena under laboratory conditions is crucial for accelerating the development of robust and durable perovskite solar cells.

1. Introduction

Recent advancements have significantly enhanced the power conversion efficiency of metal-halide perovskite solar cells (PSCs). However, the reliability of these devices under prolonged outdoor conditions remains a major obstacle to their commercialisation [1,2]. Several research institutions have undertaken outdoor exposure tests to gain insights into operational stability and identify degradation mechanisms [3–5]. PSCs exhibit different light-soaking behaviours and degradation rates under illumination, depending on their material characteristics [6]. In some cases, reversible power loss and enhancement, known as 'metastability', may occur, while in other instances, changes may be irreversible. The complexity and variability of degradation behaviours pose significant challenges in reproducing and comparing results, hindering a comprehensive understanding of PSC degradation mechanisms.

Performance measurements of devices exposed to outdoor conditions have been conducted to evaluate the energy yield of PSCs under realistic circumstances [7]. The influence of spectral irradiance on power generation was investigated for different spectra during the day [8]. Outdoor performance testing has shown that perovskite solar panels can operate for more than eight months [3], although a separate six-month experiment has shown that the open-circuit voltage maintains its initial value while the fill factor degrades [4].

For modules that underwent degradation due to field exposure or accelerated stress testing, it is important to understand the specific changes within the module that resulted in a decrease in peak power [9]. Several methods have been used to better comprehend the issues within a module. Current–voltage (I–V) curves and luminescence measurements [10] have been widely used for failure mode analysis. An analysis of the ideality factor in the I–V curve has revealed degradation associated with modified recombination mechanisms [11]. Additionally, irreversible mechanisms stem from the corrosion of the silver metal top contact, leading to the formation of silver iodide [4]. Mobile halogen ions react with the electron-transport layer under reverse bias, causing device degradation in PSCs [12]. In contrast to conventional Si solar cells, PSCs contain numerous defects and mobile ions [13]. Ion migration, which results in a reaction between migrated ions and hole-transport layers and electrodes, is considered a primary contributor to device degradation [4,14]. Given that the presence of mobile ions is a unique feature of PSCs compared to conventional Si solar cells,

* Corresponding author.
E-mail address: tayagaki-t@aist.go.jp (T. Tayagaki).

https://doi.org/10.1016/j.solmat.2024.112879
Received 8 February 2024; Received in revised form 28 March 2024; Accepted 16 April 2024
Available online 25 April 2024

mobile-ion analysis has been introduced in the literatures [15–17]. Indeed, mobile-ion concentrations increase with temperature and can influence the power reduction under illumination, as evidenced by the ion-migration current [18]. The degradation mechanism is closely linked to ion migration within the perovskite and is largely reversible overnight, though it induces hysteresis over time [4]. While light-induced ion migration can lead to material degradation, it also plays a beneficial role in defect healing [19]. Additionally, there has been discussion about oxygen-induced reversible changes in devices containing Spiro-OMeTAD, which contains numerous mobile ions [20–22].

Before examining durability and reliability, it is essential to conduct stability testing to assess the performance of PSCs in detecting slight degradations due to stressors. However, in the case of PSCs, a protocol for evaluating 'reproducible' performance has not been established due to the presence of mobile ions, which can result in metastability and make it difficult to evaluate the stabilised power conversion efficiencies. To address this issue, light–dark cycle analysis have been utilised to evaluate energy yield and compare it with real-time outdoor exposure [23]. This analysis simulates real-world temperature and illumination operating conditions [24]. The light–dark cycle is one of the test protocols proposed in International Summit on Organic PV Stability (ISOS) procedures [25]. Light–dark cycle analysis has been extended to an accelerated stress test that utilizes UV light–dark cycles, specifically designed for the metastable nature of PSCs [26]. Thus, light–dark cycle analysis and diurnal energy yield estimation can serve as valuable tools for assessing the performance of metastable PSCs.

To assess the durability and reliability of emerging PV technologies such as PSCs, it is essential to establish a testing protocol that can consistently and reproducibly demonstrate degradation. Hence, the development of accelerated testing methods that can provide a meaningful comparison with outdoor exposure tests and accurately replicate outdoor stress conditions in a laboratory environment is of paramount importance. While elevated temperatures, as part of accelerated stresses, have been widely used [27], it is essential to strike a balance as excessively harsh conditions in accelerated tests may not only accelerate the stresses observed outdoors but also induce degradation modes not typically encountered in outdoor settings, potentially leading to misleading conclusions. Therefore, there is growing interest in establishing correlations between indoor tests and outdoor field operations [28]. Novel test scenarios are needed to validate the outdoor stabilities of PSCs [29]. A thorough examination of each failure mode is necessary, along with an effort to identify the specific stressors occurring in terrestrial environments that trigger these failures [30]. Recent studies have investigated degradation modes in metal-halide perovskite PV mini-modules subjected to thermal cycling, UV exposure, or two months of outdoor exposure [10], showing that the combined test protocols might be required to reproduce the failures in the fielded modules.

Accelerated stress testing, aimed at replicating failures observed in the field, serves as a valuable tool for expending the development process. When failures are identified, module manufacturers can improve their designs, materials, and manufacturing processes to mitigate these issues. Outdoor testing of PSCs with various encapsulations has been performed and compared with indoor accelerated tests [5], contributing to the design and understanding of encapsulated PSCs capable of withstanding temperature cycling [31]. However, the degradation mechanism during outdoor exposure remains poorly understood due to its potential dependence on the unique structure and materials of each device.

In this study, we conducted field testing and investigated the degradation mechanisms of PSCs deployed in the field through mobile-ion analysis. Additionally, we compared the solar cell characteristics observed during the field tests with the results obtained from controlled indoor accelerated stress tests, which included exposure to visible light, UV irradiation, and thermal stress. We also discussed the capability to replicate outdoor degradation phenomena under laboratory conditions.

2. Experimental

Solar cells, with a F-doped tin oxide/SnO_2/perovskite/Spiro-OMeTAD/Au configuration, were fabricated for this study (Fig. 1). Prior to the perovskite layer formation, the SnO_2 layer underwent a UV ozone treatment. We fabricated $Cs_{0.05}K_{0.05}FA_{0.9}PbI_3$ (FA = $C_2H_5NH_3$) perovskites with a thickness of 400 nm. Hole-transport layers were formed on top of the perovskites by spin-coating a Spiro-OMeTAD solution containing lithium cations and 4-*tert*-butylpyridine as the dopant. Subsequently, Au contacts (5 mm × 5 mm) were formed through evaporation. Finally, the solar cells were encapsulated in glass, and the edges were sealed with UV resin. We fabricated four solar cells on glass substrates, all with nearly identical initial efficiencies.

For outdoor exposure testing, we mounted the solar cells on a perforated metal plate tilted at 20° to the horizontal, operating them near their maximum power point, assisted by a 180 Ω resistive load. A thermocouple was positioned at the rear of the device, between the device and plate. Solar irradiation was monitored by spectral integration using a spectrometer (EKO, MS-710 and MS-712) aligned with the test devices. The test site is situated at 36°N, 140°E.

For indoor testing, we employed a source-measurement unit (Keithley, 2400) to measure transient ion-migration currents, I–V curves, and maximum power [18,26]. To illuminate the fabricated devices with visible light, we used a white-light-emitting diode (WL-LED) that generated a photocurrent with an intensity approximately equivalent to one sun's intensity for AM1.5G irradiance. Furthermore, we utilised a 365-nm LED (M365L3, Thorlabs) to illuminate the fabricated devices with UV light, specifically UV-A photons. To achieve spatially uniform illumination with an illuminance of ~50 mW/cm^2, we expanded the UV-LED beam. We conducted light–dark cycling tests were for ~6 h under LED illumination, followed by storing the devices in the dark at 25 °C for ~18 h, with device temperature control facilitated by a Peltier stage. We employed maximum power point tracking (MPPT) to measure power–time curves under illumination. In these measurements, the voltage was adjusted at ~4-s intervals based on the perturb-and-observe algorithm. To determine the concentration of mobile ions, we measured the ion-migration current of the devices, following the methodology described in our previous report [17].

3. Results and discussion

3.1. Outdoor exposures

Fig. 2(a) shows the power output during typical outdoor exposure of two distinct devices. The power of these devices was estimated by monitoring voltage, calculated as $P = V^2/R_{load}$, where R_{load} represents the load resistance. One device experienced power loss within a few days, while the other maintained continuous power output for over 50 days. Notably, the power reduction over time was influenced by sunlight exposure.

Fig. 2(b) shows the amount of sunlight emitted. As the seasons changed, the daily irradiation decreased. However, the substantial power reduction indicated a potential decrease in the performance of the

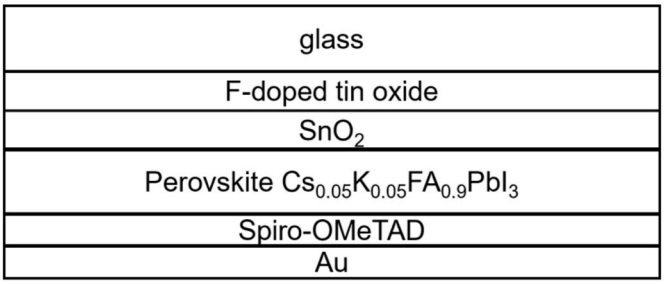

Fig. 1. Schematic of a perovskite solar cell fabricated for this study.

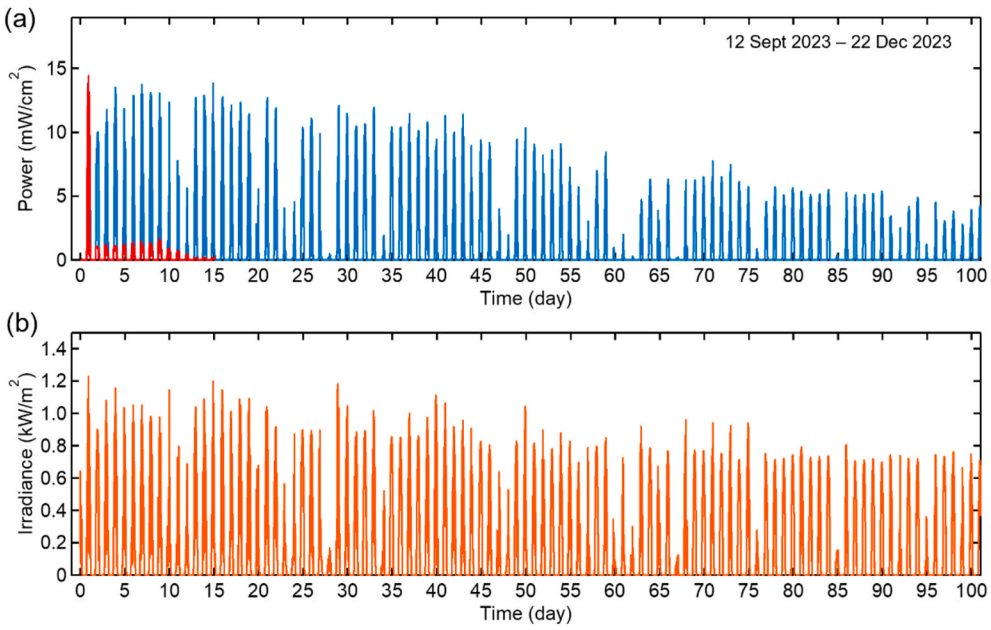

Fig. 2. Outdoor exposures: (a) Comparative power output. Red and blue lines represent power outputs of Devices #1 and #2, respectively, during outdoor exposure testing. (b) Solar irradiance over course of the outdoor exposure period.

device. Temperatures fluctuated from 40 °C during autumn daytime to −10 °C on winter nights.

Additionally, within a single day, performance varied with time. Despite similar solar irradiances, morning power output was lower than that in the afternoon. Two types of metastability have been reported: some devices exhibit power loss under illumination, while others show an increase in power under illumination [28]. There has been ongoing debate about whether light or heat is detrimental to PSCs under operating conditions [32]. A detailed performance analysis concerning irradiance and temperature shall be conducted in future studies.

3.2. Characterisation of solar cell property

Further assessment of solar cell performance focused on Device #1 before and after outdoor exposure. Fig. 3(a) and (b) show the I–V curves recorded before and after outdoor exposure, including forward and reverse sweeps, measured twice: prior to and after the power–time curve measurements under MPPT, as shown in Fig. 3(c) and (d). Post-exposure analysis revealed a notable decrease in the fill factor, indicating an increase in shunt current and/or series resistance during outdoor exposure. Several factors may have contributed to this outcome, such as enhanced number of defects, degradation of carrier transport layers, or heightened resistance, as suggested by the I–V curve analysis.

Fig. 3(c) and (d) show power–time curves observed during 6 h of WL-LED illumination at 25 °C, before and after outdoor exposure. The pre-exposure data showed a decline in power over time, while the post-exposure data showed a noticeable increase in power with illumination, with light soaking becoming predominant. As summarised in Fig. 3 (e), the energy yield during 6 h of illumination decreased after outdoor exposure, reflecting the degradation resulting from outdoor exposure. Changes in the power-time curve under illumination indicate degradation [33]. The decrease in power under illumination is due to the migration of mobile ions under illumination, which is a reversible change. The increase in power under illumination, i.e., light soaking, can also be explained by mobile ions or the filling of the trap levels by photocarriers generated by light illumination [33].

3.3. Mobile-ion analysis

To gain insight into the mechanism behind metastability and degradation, we conducted transient ion-migration current measurements (Fig. 4(a)). We applied a forward bias of 1.5 V to the device for 30 s to perturb the initial distribution of mobile ions in the dark conditions. Subsequently, the device was set to zero-bias conditions to induce the backward propagation of ions. Fig. 4(b) shows the current–time curves of the transient ion-migration current measurements conducted before outdoor exposure. To account for metastability, these measurements were performed twice: before and after 6 h of WL-LED illumination. Following WL-LED illumination, the ion-migration current increased, consistent with previous reports [17,18].

Fig. 4(c) shows the current–time curves of the transient ion-migration current measurements after outdoor exposure. Notably, there was an increase in concentration following illumination, which diminished when the device was kept in the dark.

The mobile-ion concentration (N_{ion}) was estimated using the following equation

$$N_{ion} = \frac{1}{Adq}\int_{t_1}^{t_2} I_{IMC}(t)dt \tag{1}$$

where $I_{\mathrm{IMC}}(t)$ presents the transient ion-migration current; t denotes time; t_1 and t_2 denote the limits of time integration; A and d represent the area and thickness of the perovskite layer, respectively, and q stands for the elementary charge. We calculated fast, slow, and total mobile-ion concentrations using the transient currents over the time ranges t_1–t_2 of 30–33, 33–80, and 30–80 s, respectively. A detailed identification of the mobile-ion species goes beyond the scope of this study. Fig. 4(d) summarises the ion concentrations for the results presented in Fig. 4(b) and (c). The concentration of slow mobile ions increased after illumination. Notably, there was a pronounced increase in the ion-migration current after illumination in the devices subjected to outdoor exposure. This suggests the possibility of an increased presence of deep traps, which are activated by light illumination, after exposure to outdoor conditions. This finding underscores potential changes in the microstructure of perovskite materials due to outdoor exposure, particularly the formation of deep-level traps that could significantly influence the

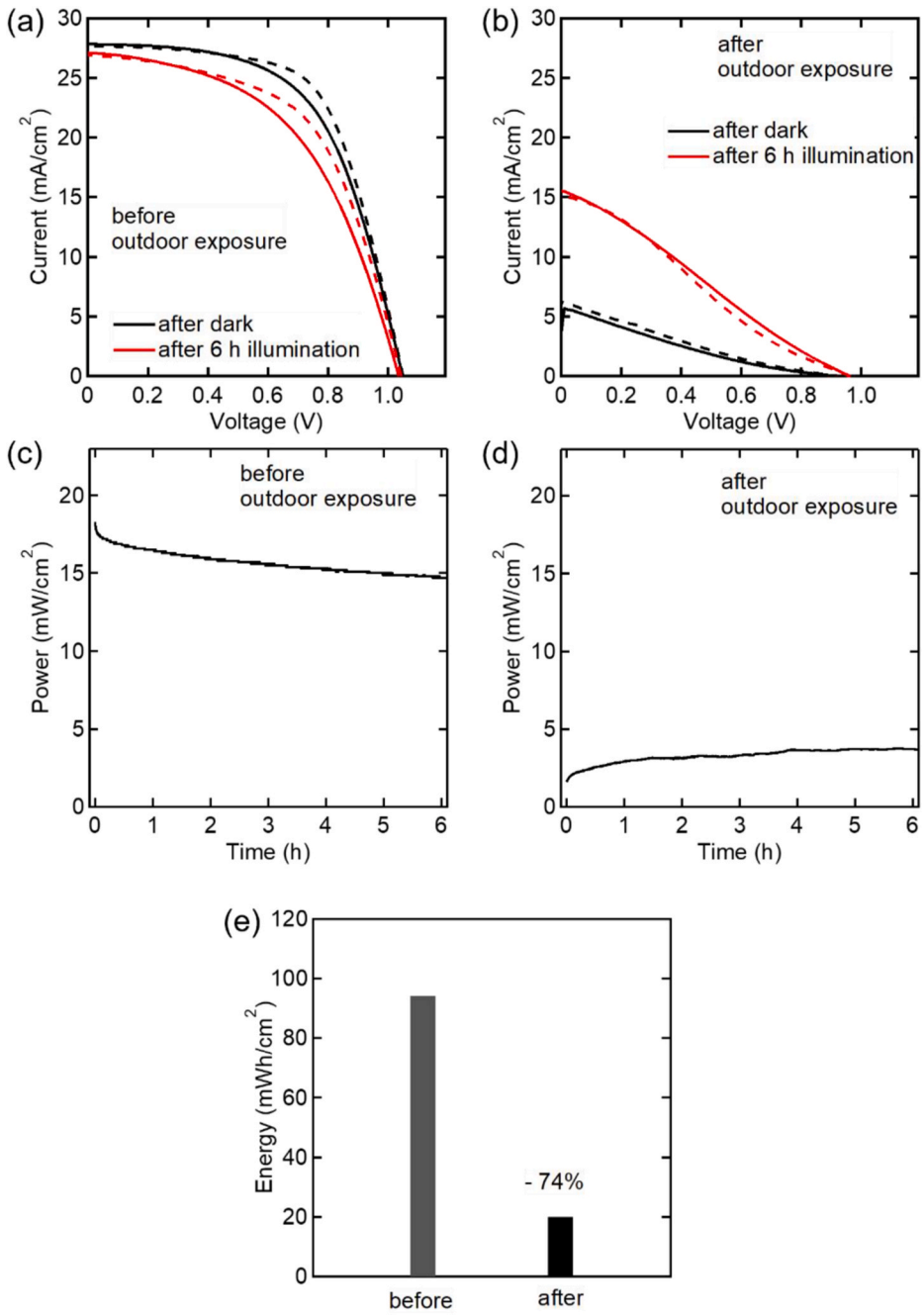

Fig. 3. Characterisation at outdoor exposure test: (a) I–V curves before and (b) after outdoor exposure. Curves before and after 6 h of WL-LED illumination under MPPT were plotted. Solid and broken curves were measured for forward and reverse voltage sweep, respectively. (c) Power–time curves during 6 h of WL-LED illumination, before and (d) after outdoor exposure. (e) Calculated energy yield for 6 h of WL-LED illumination, before and after outdoor exposure.

operational stability and long-term performance of these solar cells.

Assuming that deep-level defects cannot migrate under the applied voltage, it is postulated that illumination activates traps to shallower-level mobile defects, increasing the number of mobile ions after outdoor exposure. This interpretation implies that outdoor exposure leads to degradation due to an increase in deep-level traps. The defect thermal activation energy is approximately the depth of defect state energy level relative to the valence or conduction bands of the perovskite [34]. Therefore, the thermal activation energy of the ion-migration current was evaluated from temperature-dependence measurements [18]. First, the ion-migration currents were measured at different temperatures. Then, the concentrations calculated using the ion-migration current are plotted as a function of temperature. By fitting the ion concentration that increased with temperature by $N(T) = N_0 \exp\left(-\frac{E_a}{T}\right)$, the thermal activation energy E_a as 0.4–0.5 eV was well obtained. A previous study reported an activation energy of ~0.40 eV for transport property in a device with Spiro-OMeTAD [35], which is similar to the activation energy of the defects in this work. However, ion migration related to Spiro-OMeTAD is believed to be influenced by elevated temperatures. Therefore, despite differences in device structures, the effect of Spiro-OMeTAD is not likely, and the ion movement observed in this work can primarily be attributed to perovskite defects. The detailed analysis of the defect features will be shown subsequently.

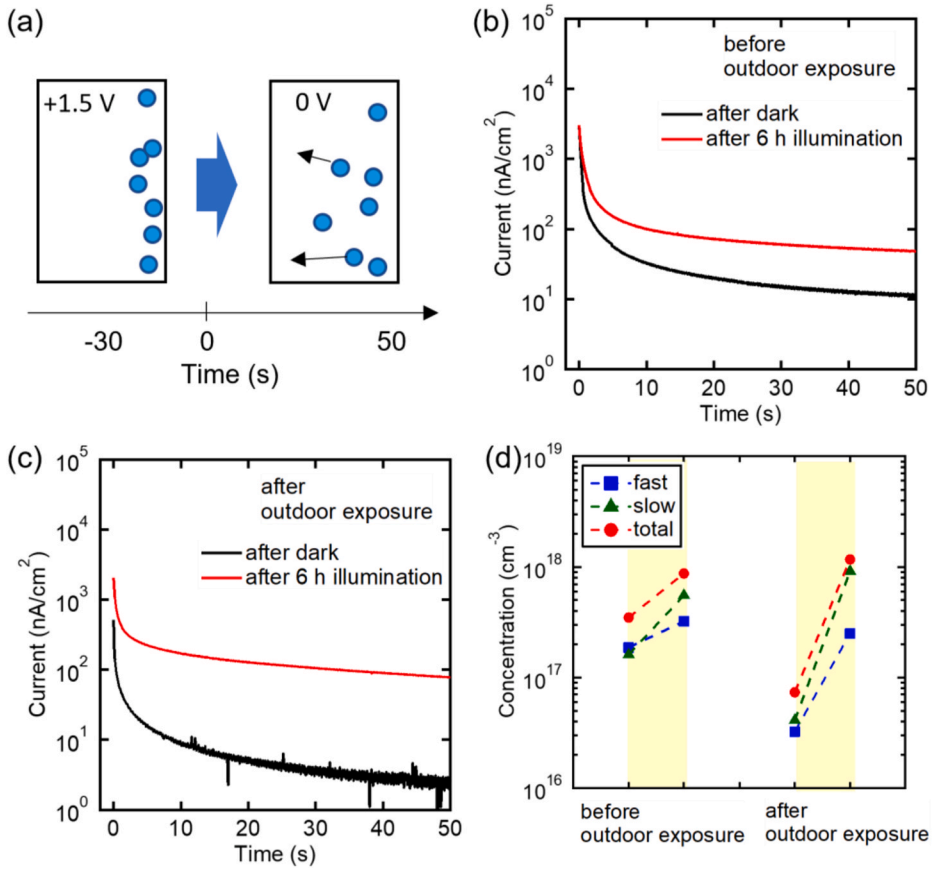

Fig. 4. Ion-migration currents at outdoor exposure test: (a) Schematic of ion-migration currents. (b) Ion-migration currents in device before and (c) after outdoor exposure, with both before and after WL-LED illumination. (d) Calculated concentrations of mobile ions within device, before and after outdoor exposure.

3.4. Accelerated stress testing

To understand the degradation mechanism induced by outdoor exposure, we conducted accelerated stress tests, which included visible-light illumination, UV irradiation, and dark storage at elevated temperatures. Below, we present the results for the device with the highest durability among the four samples tested.

3.4.1. Visible-light illumination

We conducted a light illumination test at 60 °C using WL-LED illumination. Fig. 5(a) shows a schematic of the testing procedure, involving 116 h of LED illumination at elevated temperatures. After subjecting the device to light–dark cycles to assess its stability, we conducted the light illumination test at 60 °C using WL-LED illumination, following additional light–dark cycles. The device operated under MPPT during WL-LED illumination. Throughout the light–dark cycle and before and after 116 h of WL-LED illumination, we evaluated the device using I–V curve measurements, ion-migration current measurements, as well as outdoor exposed devices.

Fig. 5(b) and (c) show the I–V curves at 25 °C and 60 °C during light–dark cycles before 116 h of WL-LED illumination. Hereafter, the results of the second cycle are shown as a representative curve at 60 °C. The device exhibited performance degradation during light–dark cycles. Fig. 5(d) and (e) show the I–V curves at 25 °C and 60 °C during light–dark cycles after WL-LED illumination. The device demonstrated a recovery of performance degradation after 6 h of WL-LED illumination, indicating that the light-soaking effect prevailed. Fig. 5(f) summarises the power–time curves for 6 h of WL-LED illumination. Prior to visible-light illumination at elevated temperatures, the device experienced power loss during illumination. However, after 116 h of WL-LED illumination, the device exhibited increased power under illumination. This behaviour was similarly observed in a device exposed to outdoor conditions. Fig. 5(g) summarises the energy yield of 6 h of WL-LED during visible-light illumination testing.

Fig. 6(a)–(d) show the ion-migration currents corresponding to Fig. 5 (b)–(d). The ion-migration currents increased at 60 °C, attributed to thermal activation [18]. However, after 116 h of WL-LED exposure, the current decreased, particularly at 25 °C. Fig. 6(e) summarises the calculated concentrations of total mobile ions during visible-light illumination testing before and after LED illumination. For simplicity, the concentration was determined from the transient currents measured over a time range (t_1–t_2) of 30–80 s. Each light cycle altered the mobile-ion concentration, and the modification during light–dark cycles also changed after 116 h of LED illumination. The thermal activation energy of the ion-migration current was evaluated to be ~0.3 eV from temperature-dependence measurements conducted after the testing.

3.4.2. Thermal stress

We conducted thermal stress tests in the dark to compare the effects of thermal stress. Fig. 7(a) outlines the schematic testing procedures, where WL-LED was turned off during 116 h of storage at 60 °C.

Fig. 7(b) and (c) show the I–V curves at 25 °C and 60 °C during light–dark cycles, before subjecting the device to 116 h of thermal stress. Fig. 7(d) and (e) show the I–V curves at 60 °C and 25 °C during light–dark cycles after the thermal stress. The device exhibited a decrease in the fill factor during testing. Even after the thermal stress, the I–V curves for the forward and reverse voltage sweeps remained unchanged after 6 h of WL-LED illumination, indicating that the light-soaking effect was less pronounced at elevated temperatures. Fig. 7(f) shows the power–time curves for 6 h of WL-LED illumination. The power reduction was not as significant, and light soaking was observed to a lesser extent, particularly at 25 °C after thermal stress testing. Fig. 7(g) summarises

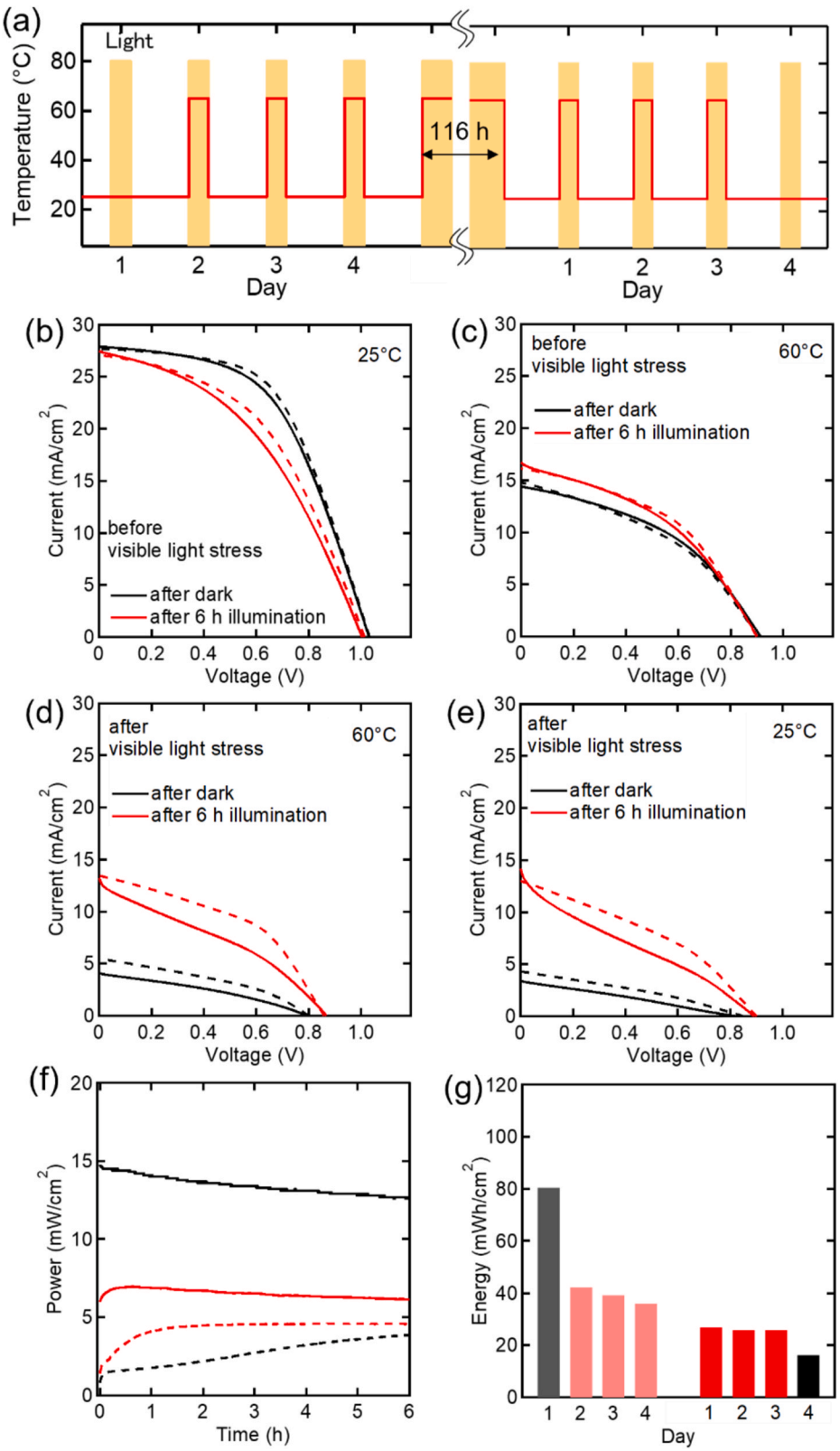

Fig. 5. Characterisation at visible-light illumination testing: (a) Schematic of testing procedure. (b) I–V curves at 25 °C and (c) 60 °C during light–dark cycles before 116 h of WL-LED illumination, with both before and after 6 h of WL-LED illumination. Solid and broken curves were measured for forward and reverse voltage sweep, respectively. (d) I–V curves at 60 °C and (e) 25 °C during light–dark cycles after 116 h of WL-LED illumination. (f) Power–time curves during 6 h of WL-LED illumination at 25 °C (black) and 60 °C (red) before (solid) and after (broken) 116 h of WL-LED illumination. (g) Calculated energy yield for 6 h of WL-LED illumination, during visible-light illumination tests.

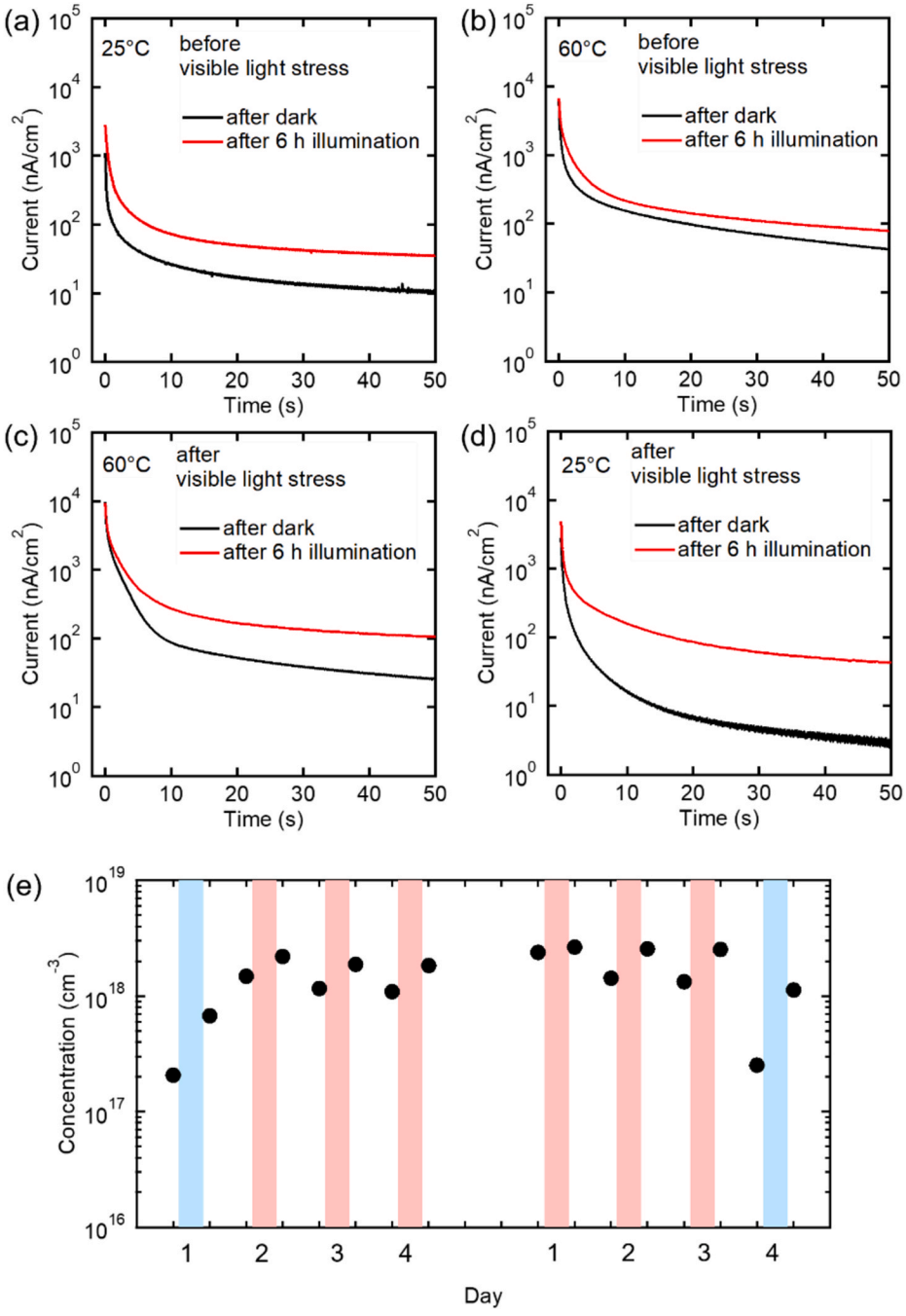

Fig. 6. Ion-migration currents at visible-light illumination testing: (a) Ion migration currents at 25 °C and (b) 60 °C during light–dark cycles in device before 116 h of WL-LED illumination, with both before and after 6 h of WL-LED illumination. (c) Ion-migration currents at 60 °C and (d) 25 °C during light–dark cycles after 116 h of WL-LED illumination. (e) Calculated concentrations of mobile ions, during visible-light illumination tests.

the calculated energy yield during thermal stress testing.

Fig. 8(a)–(d) show the ion-migration currents corresponding to Fig. 7 (b)–(d). The modification in mobile-ion concentration during light–dark cycles is similar to that shown in Fig. 6. Fig. 8(e) shows the calculated concentrations of mobile ions during thermal stress testing. The increase in mobile-ion concentration during 6 h of WL-LED illumination at 60 °C was significant, contrasting the case of 25 °C. This is in contrast to the results of visible-light illumination stress, where the change at 60 °C was smaller than at 25 °C. These results indicate that thermal activation of defects may vary depending on the damage caused by each type of stress. Indeed, the thermal activation energy of the ion-migration current was evaluated to be ~0.2 eV from temperature-dependence measurements. This value significantly differs from those observed in devices exposed to outdoor conditions and visible-light illumination. This indicates that outdoor stress is not primarily induced by elevated temperatures. However, the change in mobile-ion concentration was substantial for dark storage at elevated temperatures compared to visible-light illumination at elevated temperatures. This suggests that damage to the perovskite absorber may be partially mitigated by light illumination at elevated temperatures [19].

3.4.3. *UV irradiation*

We conducted a UV irradiation test using a 365 nm UV LED to simulate environmental stress [26]. Fig. 9(a) shows the schematic testing procedures, where UV-light–dark cycles and 284 h of UV irradiation were conducted. The device operated under MPPT during UV

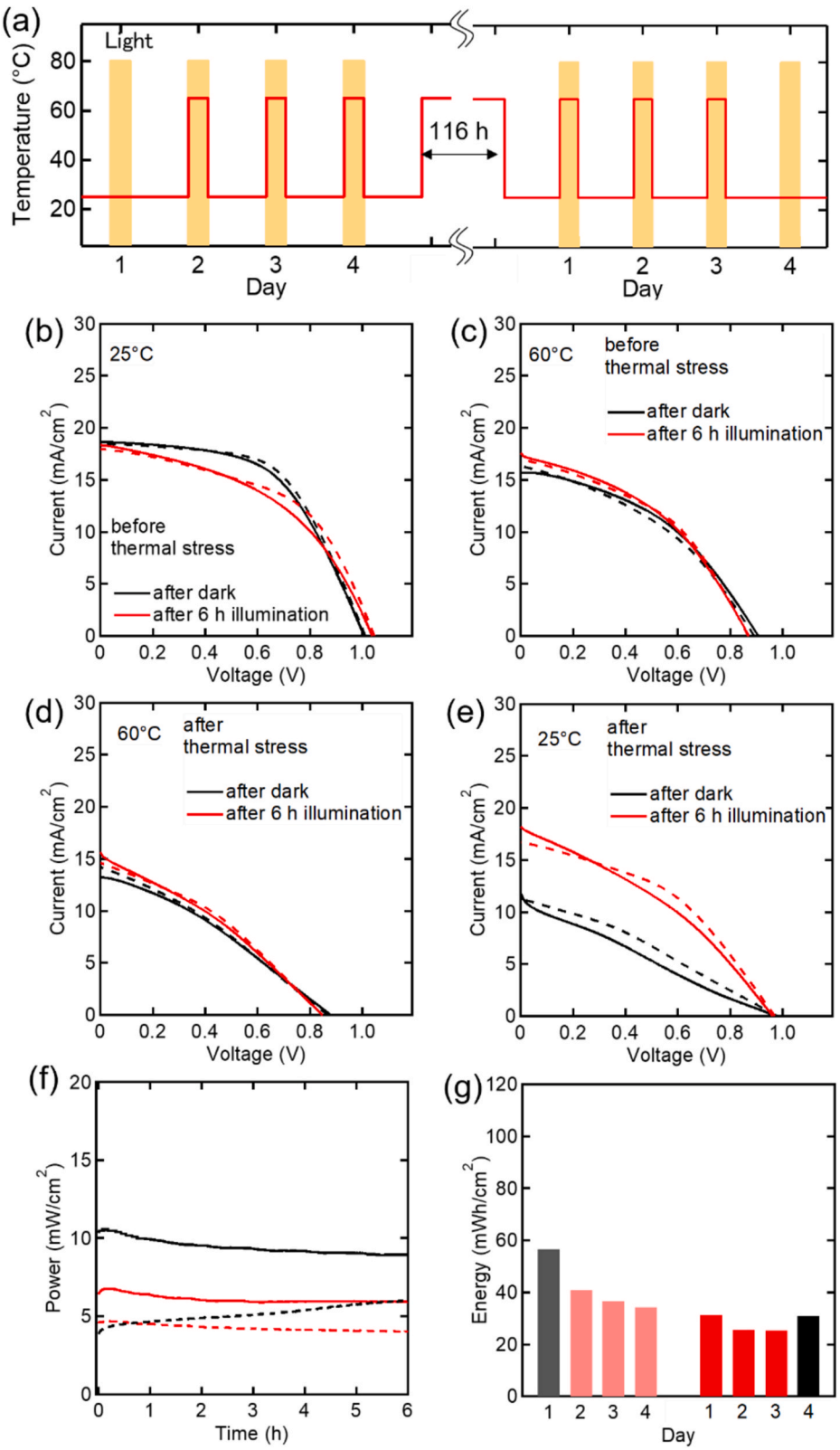

Fig. 7. Characterisation at thermal stress testing: (a) Schematic of testing procedure. (b) I–V curves at 25 °C and (c) 60 °C during light–dark cycles before 116 h of thermal stress, with both before and after 6 h of WL-LED illumination. Solid and broken curves are measured for forward and reverse voltage sweep, respectively. (d) I–V curves at 60 °C and (e) 25 °C during light–dark cycles after thermal stress. (f) Power–time curves during 6 h of WL-LED illumination at 25 °C (black) and 60 °C (red) before (solid) and after (broken) thermal stress. (g) Calculated energy yield for 6 h of WL-LED illumination, during thermal stress tests.

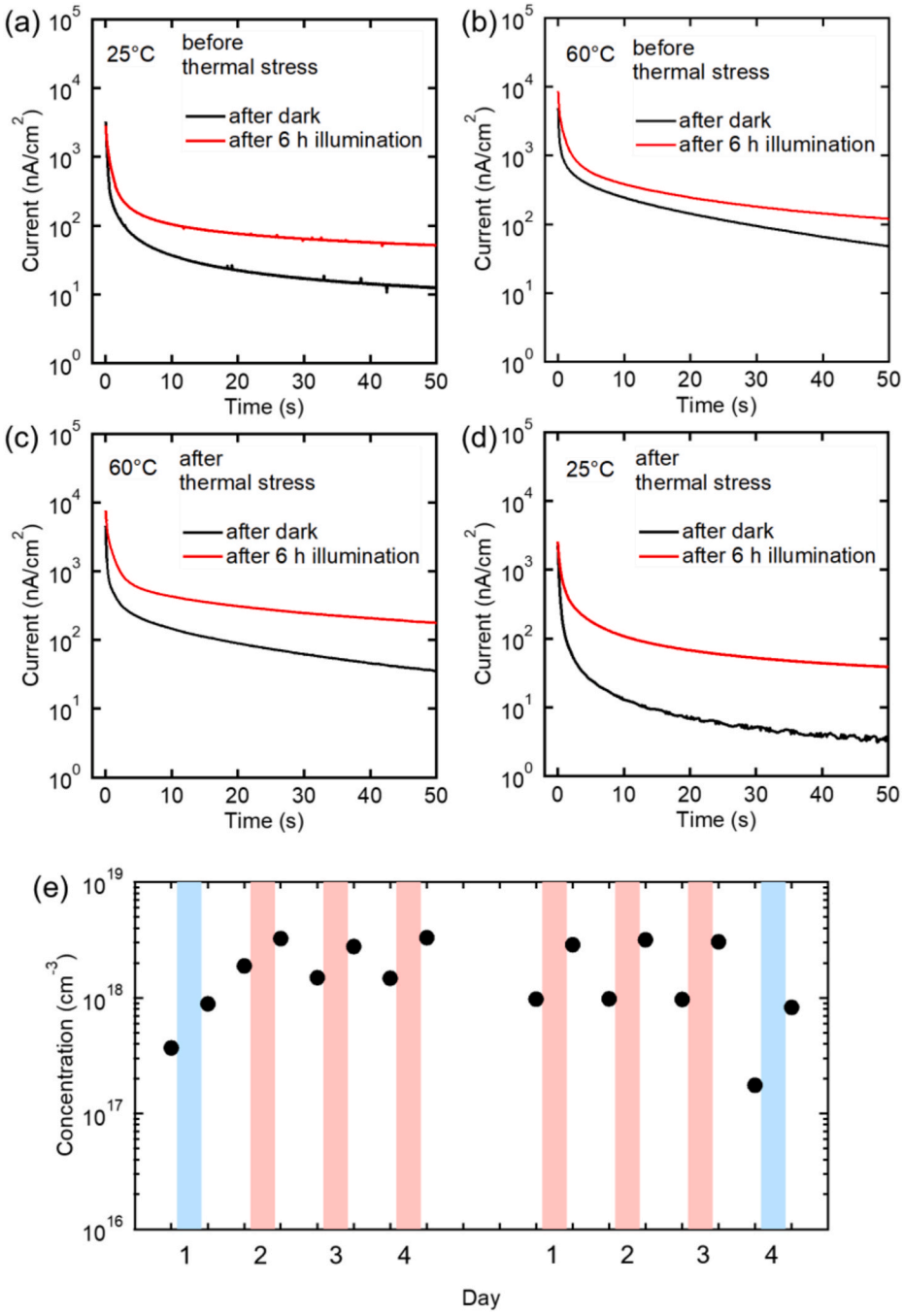

Fig. 8. Ion-migration currents at thermal stress testing: (a) Ion-migration currents at 25 °C and (b) 60 °C during light–dark cycles before 116 h of thermal stress. (c) Ion-migration currents at 60 °C and (d) 25 °C during light–dark cycles after 116 h of thermal stress. (e) Calculated concentrations of mobile ions, during thermal stress tests.

irradiation.

Fig. 9(b) and (c) show the I–V curves at 25 °C and 60 °C during light–dark cycles before subjecting the device to 284 h of UV irradiation. The increase in current during light–dark cycles at 60 °C indicates the appearance of metastability, i.e., the light-soaking effect. Fig. 9(d) and (e) show the I–V curves at 60 °C and 25 °C during light–dark cycles after the UV irradiation. The current after dark storage decreased significantly both at 60 °C and 25 °C. Fig. 9(f) shows the power–time curves for 6 h of UV-LED illumination. Light soaking was evident after outdoor exposure. Fig. 9(g) summarises the energy before and after outdoor exposure. Note that the energy data on the 4th day prior to UV irradiation stress was not displayed due to instrument errors.

Fig. 10(a)–(d) show the ion-migration currents corresponding to Fig. 9(b)–(d). The current after dark storage decreased significantly both at 25 °C and 60 °C after 284 h of UV-LED illumination. Fig. 10(e) shows the calculated concentrations of mobile ions during UV irradiation. While the solar cells used were not degraded by UV-LED illumination at 45 °C in a previous study, the impact of UV irradiation became more pronounced at elevated temperatures (60 °C). This suggests that the degradation under UV irradiation may be related to mobile ions, as the associated mobile defects may increase at elevated temperatures. The thermal activation energy of the ion-migration current was evaluated as 0.3–0.4 eV from temperature-dependence measurements, indicating the formation of deep-level traps. This indicates that UV irradiation at

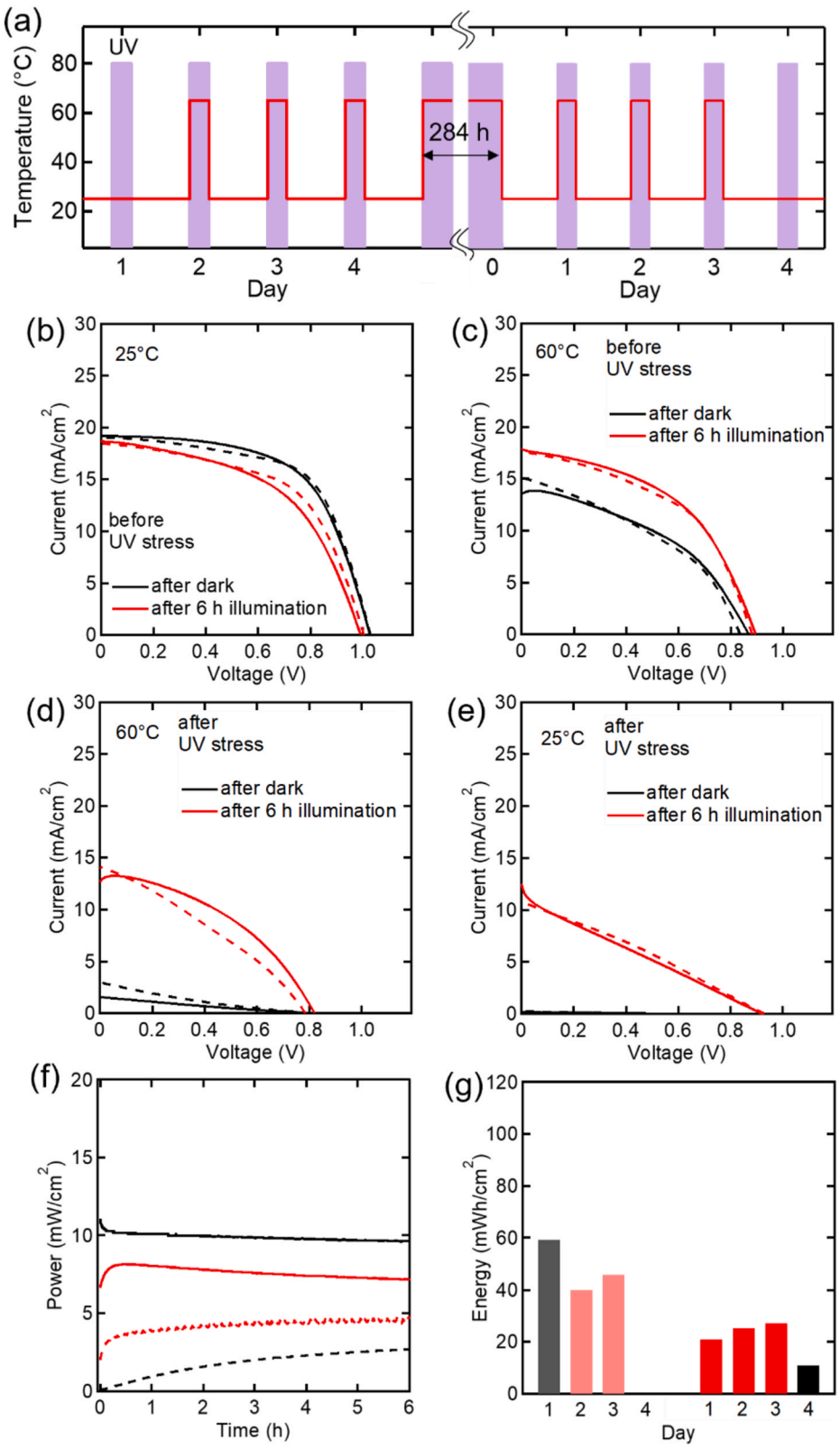

Fig. 9. Characterisation at UV irradiation testing: (a) Schematic of testing procedure. (b) I–V curves at 25 °C and (c) 60 °C during light–dark cycles before 284 h of UV irradiation, with both before and after 6 h of WL-LED illumination. (d) I–V curves at 60 °C and (e) 25 °C during light–dark cycles after UV irradiation. (f) Power–time curves during 6 h of WL-LED illumination at 25 °C (black) and 60 °C (red) before (solid) and after (broken) after 284 h of UV irradiation. (g) Calculated energy yield for 6 h of UV-LED illumination, during UV irradiation tests.

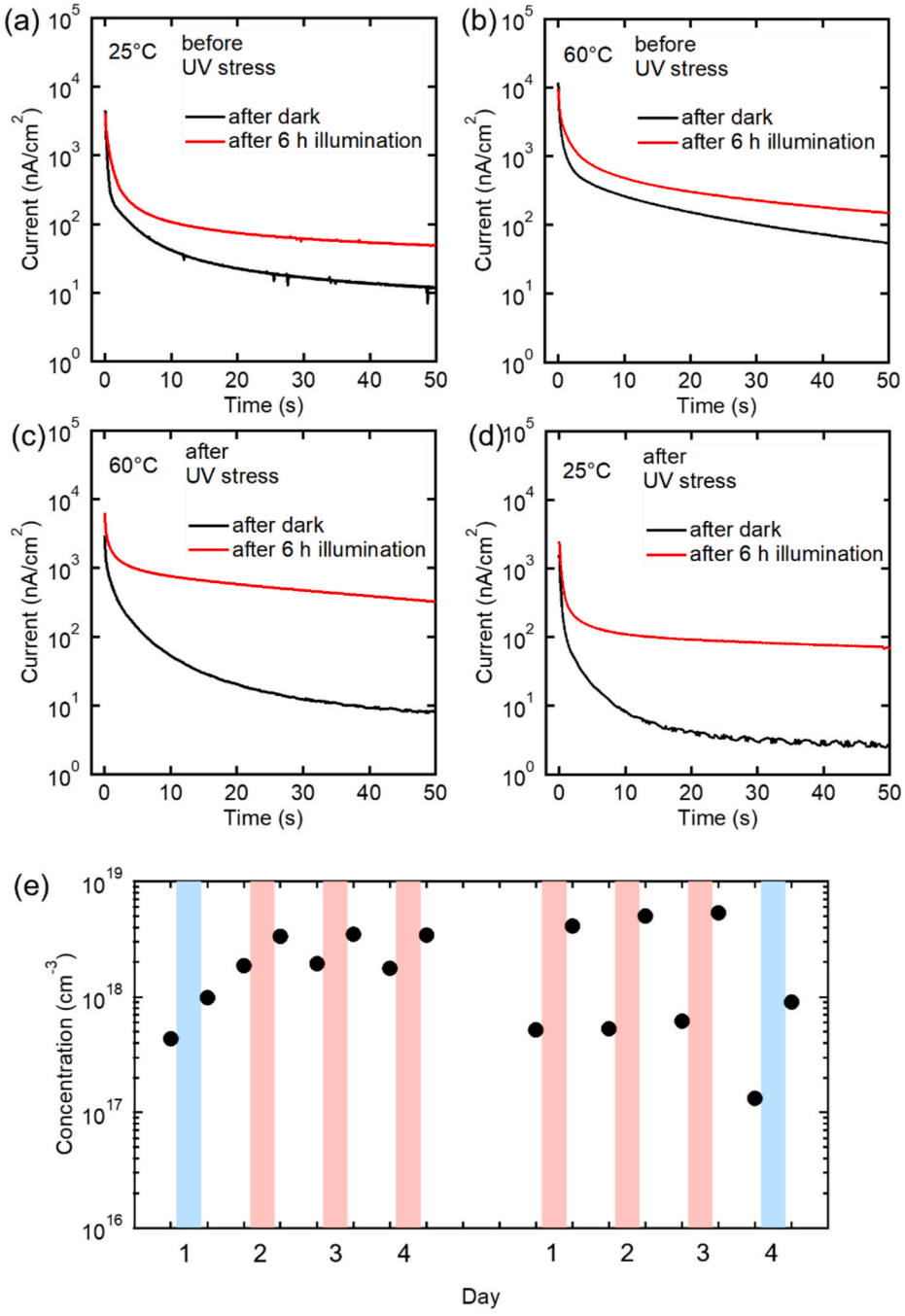

Fig. 10. Ion-migration currents at UV irradiation testing: (a) Ion-migration currents at 25 °C and (b) 60 °C during light–dark cycles before 284 h of UV irradiation. (c) Ion-migration currents at 60 °C and (d) 25 °C during light–dark cycles after UV irradiation. (e) Calculated concentrations of mobile ions, during UV irradiation tests.

elevated temperatures induces degradation similar to that experienced during outdoor exposure. A longer irradiation time of 284 h was not the primary cause of significant modification under UV irradiation. We confirmed that almost the same results as those shown in Figs. 4 and 5 were obtained even when the WL-LED illumination was extended to 284 h.

3.5. *Comparison of outdoor exposure and indoor accelerated stress testing*

The indoor accelerated stress testing was performed under three conditions, resulting in changes in I–V curves and decrease in fill factors similar to changes at outdoor exposure. The changes in power-time curves are also qualitatively similar between outdoor exposure and indoor stress tests. Prior to the stress tests, the device exhibited reduced power under illumination; however, after testing, there was an increase in power under illumination. Stress tests significantly modified the concentration of mobile ions. Thus, the characteristics of the solar cells resembled those of devices that had undergone outdoor exposure. Under indoor test conditions, the properties of mobile ions are almost similar, but UV irradiation stress in particular causes degradation similar to outdoor exposure. The thermal activation energy of the ion-migration current indicated that deep-level traps were formed under UV irradiation. This study revealed that UV irradiation at elevated temperatures induces degradation similar to that experienced during outdoor exposure, emphasising its significance as a critical stress factor for replicating the degradation phenomena of PSCs in actual outdoor environments.

These insights are crucial for understanding the endurance of these cells and for developing strategies to enhance their durability for real-world applications. The ability to replicate outdoor degradation phenomena under laboratory conditions is a crucial step towards accelerating the development of robust and durable PSC modules [36,37].

It is worth noting that testing under UV irradiation at elevated temperatures is not a part of the standardised tests for conventional PV modules, such as IEC 61215 [38]. While some studies have reported PSCs passing the IEC 61215 test designed for conventional PV modules such as c-Si, the applicability of these conditions to PSCs remains unclear. In the case of the PSCs examined in this study, the observed degradation may be linked to defect modification within the perovskite layer rather than encapsulant and packaging degradation, which is observed in more mature Si and thin-film modules. Thus, mobile-ion analysis, reflecting the formation of mobile defects in the perovskite layer, shows significant changes due to various stressors.

Stability testing is a paramount concern in the development of accelerated stress tests for metastatic PSCs. Without it, evaluating performance degradation becomes challenging. Light–dark cycle analysis presents a potential test protocol that can help determine whether performance degradation is reversible or irreversible. Moreover, the metastability of PSCs may be connected to mobile defects and their responses to stressors such as light and heat. This bears some resemblance to light and elevated temperature-induced degradation (LETID), a recently observed degradation mode in Si PVs [39,40], which is explained by a three-state model [37]; the BO defect plays an important role; a three-states model is assumed to account for metastability and regeneration [41]. Similar to LETID, a thorough examination of related defects, likely arising from iodide-related defects, will be the next step in comprehending the degradation mechanisms of PSCs. To achieve more stable, durable, and reliable PV technology, future device designs will require more advanced passivation techniques for detrimental defects [42–48].

4. Conclusion

In this study, field tests were performed to assess the durability of PSCs under real-world conditions. While one device maintained power generation for over a month, the other experienced a significant power loss. A comprehensive failure analysis was carried out to identify the specific degradation mechanisms induced by outdoor exposure. This analysis revealed a significant alteration in the ion-migration current response of the devices after exposure, indicating that modifications in mobile ions and the formation of defects within the perovskite layer are likely the primary cause of degradation. Additionally, we compared the solar cell characteristics observed during the field test with the results of controlled indoor accelerated stress tests, including exposure to visible light, UV irradiation, and thermal stress. Our findings highlight that the degradation patterns induced by UV irradiation at elevated temperatures closely resemble those caused by outdoor stress. The ability to replicate outdoor degradation phenomena under laboratory conditions is crucial for accelerating the development of robust and durable PSC modules.

CRediT authorship contribution statement

Takeshi Tayagaki: Writing – review & editing, Writing – original draft, Investigation, Data curation, Conceptualization. **Sayaka Hirooka:** Investigation, Data curation. **Haruka Kobayashi:** Investigation, Data curation. **Kohei Yamamoto:** Writing – review & editing, Resources. **Takurou N. Murakami:** Writing – review & editing, Resources, Funding acquisition. **Masahiro Yoshita:** Writing – review & editing, Investigation, Funding acquisition.

Declaration of competing interest

The authors declare that they have no known competing financial interests or personal relationships that could have appeared to influence the work reported in this paper.

Data availability

The data that has been used is confidential.

Acknowledgements

This work was partially supported by the New Energy and Industrial Technology Development Organization (NEDO, JPNP21016) under the Ministry of Economy, Trade and Industry (METI).

References

[1] C.C. Boyd, R. Cheacharoen, T. Leijtens, M.D. McGehee, Understanding degradation mechanisms and improving stability of perovskite photovoltaics, Chem. Rev. 119 (2019) 3418–3451, https://doi.org/10.1021/acs.chemrev.8b00336.
[2] W. Xiang, S. Liu, W. Tress, A review on the stability of inorganic metal halide perovskites: challenges and opportunities for stable solar cells, Energy Environ. Sci. 14 (2021) 2090–2113, https://doi.org/10.1039/d1ee00157d.
[3] S. Pescetelli, A. Agresti, G. Viskadouros, S. Razza, K. Rogdakis, I. Kalogerakis, E. Spiliarotis, E. Leonardi, P. Mariani, L. Sorbello, M. Pierro, C. Cornaro, S. Bellani, L. Najafi, B. Martín-García, A.E. Del Rio Castillo, R. Oropesa-Nuñez, M. Prato, S. Maranghi, M.L. Parisi, A. Sinicropi, R. Basosi, F. Bonaccorso, E. Kymakis, A. Di Carlo, Integration of two-dimensional materials-based perovskite solar panels into a stand-alone solar farm, Nat. Energy 7 (2022) 597–607, https://doi.org/10.1038/s41560-022-01035-4.
[4] M. De Bastiani, E. Van Kerschaver, Q. Jeangros, A. Ur Rehman, E. Aydin, F. H. Isikgor, A.J. Mirabelli, M. Babics, J. Liu, S. Zhumagali, E. Ugur, G.T. Harrison, T. G. Allen, B. Chen, Y. Hou, S. Shikin, E.H. Sargent, C. Ballif, M. Salvador, S. De Wolf, Toward stable Monolithic perovskite/silicon tandem photovoltaics: a six-month outdoor performance study in a hot and humid climate, ACS Energy Lett. 6 (2021) 2944–2951, https://doi.org/10.1021/acsenergylett.1c01018.
[5] Q. Emery, M. Remec, G. Paramasivam, S. Janke, J. Dagar, C. Ulbrich, R. Schlatmann, B. Stannowski, E. Unger, M. Khenkin, Encapsulation and outdoor testing of perovskite solar cells: comparing industrially relevant process with a simplified lab procedure, ACS Appl. Mater. Interfaces 14 (2022) 5159–5167, https://doi.org/10.1021/acsami.1c14720.
[6] K. Domanski, B. Roose, T. Matsui, M. Saliba, S.H. Turren-Cruz, J.P. Correa-Baena, C.R. Carmona, G. Richardson, J.M. Foster, F. De Angelis, J.M. Ball, A. Petrozza, N. Mine, M.K. Nazeeruddin, W. Tress, M. Grätzel, U. Steiner, A. Hagfeldt, A. Abate, Migration of cations induces reversible performance losses over day/night cycling in perovskite solar cells, Energy Environ. Sci. 10 (2017) 604–613, https://doi.org/10.1039/c6ee03352k.
[7] M. Jošt, B. Lipovšek, B. Glažar, A. Al-Ashouri, K. Brecl, G. Matič, A. Magomedov, V. Getautis, M. Topič, S. Albrecht, Perovskite solar cells go outdoors: field testing and temperature effects on energy yield, Adv. Energy Mater. 10 (2020) 2000454, https://doi.org/10.1002/aenm.202000454.
[8] M. Huang, C. Shou, J. Sun, Q. Shen, C. Huang, H. Peng, S. Jin, H. He, Perovskite solar module outdoor field testing and spectral irradiance effects on power generation, Phys. Status Solidi Rapid Res. Lett. 2200220 (2022) 2–7, https://doi.org/10.1002/pssr.202200220.
[9] J.H. Wohlgemuth, Failure analysis tools, in: Photovolt. Modul. Reliab., John Wiley & Sons Ltd., Hoboken, 2020, pp. 127–150, https://doi.org/10.1002/9781119459019.ch5.
[10] J.W. Schall, A. Glaws, N.Y. Doumon, T.J. Silverman, M. Owen-Bellini, K. Terwilliger, M.A. Uddin, P. Rana, J.J. Berry, J. Huang, L.T. Schelhas, D.B. Kern, Accelerated stress testing of perovskite photovoltaic modules: differentiating degradation modes with electroluminescence imaging, Sol. RRL 2300229 (2023) 2300229, https://doi.org/10.1002/solr.202300229.
[11] E. Velilla, F. Jaramillo, I. Mora-Seró, High-throughput analysis of the ideality factor to evaluate the outdoor performance of perovskite solar minimodules, Nat. Energy 6 (2021) 54–62, https://doi.org/10.1038/s41560-020-00747-9.
[12] I.E. Gould, C. Xiao, J.B. Patel, M.D. McGehee, In-operando characterization of P-I-N perovskite solar cells under reverse bias, in: Conf. Rec. IEEE Photovolt, Spec. Conf., 2021, pp. 1365–1367, https://doi.org/10.1109/PVSC43889.2021.9518723.
[13] Y. Yuan, J. Chae, Y. Shao, Q. Wang, Z. Xiao, A. Centrone, J. Huang, Photovoltaic switching mechanism in lateral structure hybrid perovskite solar cells, Adv. Energy Mater. 5 (2015) 1500615, https://doi.org/10.1002/aenm.201500615.
[14] Y. Zhao, W. Zhou, H. Tan, R. Fu, Q. Li, F. Lin, D. Yu, G. Walters, E.H. Sargent, Q. Zhao, Mobile-ion-induced degradation of organic hole-selective layers in perovskite solar cells, J. Phys. Chem. C 121 (2017) 14517–14523, https://doi.org/10.1021/acs.jpcc.7b04684.
[15] O.S. Game, G.J. Buchsbaum, Y. Zhou, N.P. Padture, A.I. Kingon, Ions matter: description of the anomalous electronic behavior in methylammonium lead halide perovskite devices, Adv. Funct. Mater. Adv. Funct. Mater. 27 (2017) 1606584, https://doi.org/10.1002/adfm.201606584.

[16] Y. Deng, S. Xu, S. Chen, X. Xiao, J. Zhao, J. Huang, Defect compensation in formamidinium–caesium perovskites for highly efficient solar mini-modules with improved photostability, Nat. Energy 6 (2021) 633–641, https://doi.org/10.1038/s41560-021-00831-8.
[17] T. Tayagaki, A. Kogo, C. Mcdonald, V. Svrcek, T. Matsui, Transient analysis of ion-migration current for degradation diagnostics of perovskite solar cells, IEEE J. Photovoltaics 12 (2022) 1170–1174, https://doi.org/10.1109/JPHOTOV.2022.3189794.
[18] T. Tayagaki, K. Yamamoto, T.N. Murakami, M. Yoshita, Temperature-dependent ion migration and mobile-ion-induced degradation of perovskite solar cells under illumination, Sol. Energy Mater. Sol. Cells 257 (2023) 112387, https://doi.org/10.1016/j.solmat.2023.112387.
[19] S.G. Motti, D. Meggiolaro, A.J. Barker, E. Mosconi, C.A.R. Perini, J.M. Ball, M. Gandini, M. Kim, F. De Angelis, A. Petrozza, Controlling competing photochemical reactions stabilizes perovskite solar cells, Nat. Photonics 13 (2019) 532–539, https://doi.org/10.1038/s41566-019-0435-1.
[20] B. Purev-Ochir, X. Liu, Y. Fujita, D. Semba, T.B. Raju, G. Tumen-Ulzii, A. Wachi, H. Sato, T. Matsushima, C. Adachi, Oxygen-induced reversible degradation of perovskite solar cells, Sol. RRL 7 (2023) 2300127, https://doi.org/10.1002/solr.202300127.
[21] L. Huang, Z. Ge, X. Zhang, Y. Zhu, Oxygen-induced defect-healing and photo-brightening of halide perovskite semiconductors: science and application, J. Mater. Chem. A 9 (2021) 4379–4414, https://doi.org/10.1039/d0ta10946k.
[22] D. Shin, F. Zu, N. Koch, Reversible oxygen-induced p -doping of mixed-cation halide perovskites, Apl. Mater. 9 (2021) 081104, https://doi.org/10.1063/5.0056346.
[23] D. Cunningham, M. Rubcich, D. Skinner, Cadmium telluride PV module manufacturing at BP solar, Prog. Photovoltaics Res. Appl. 10 (2002) 159–168, https://doi.org/10.1002/pip.417.
[24] W. Tress, K. Domanski, B. Carlsen, A. Agarwalla, E.A. Alharbi, M. Graetzel, A. Hagfeldt, Performance of perovskite solar cells under simulated temperature-illumination real-world operating conditions, Nat. Energy 4 (2019) 568–574, https://doi.org/10.1038/s41560-019-0400-8.
[25] M.V. Khenkin, E.A. Katz, A. Abate, G. Bardizza, J.J. Berry, C. Brabec, F. Brunetti, V. Bulović, Q. Burlingame, A. Di Carlo, R. Cheacharoen, Y.B. Cheng, A. Colsmann, S. Cros, K. Domanski, M. Dusza, C.J. Fell, S.R. Forrest, Y. Galagan, D. Di Girolamo, M. Grätzel, A. Hagfeldt, E. von Hauff, H. Hoppe, J. Kettle, H. Köbler, M.S. Leite, S. Frank, Liu, Y.L. Loo, J.M. Luther, C.Q. Ma, M. Madsen, M. Manceau, M. Matheron, M. McGehee, R. Meitzner, M.K. Nazeeruddin, A.F. Nogueira, Ç. Odabaşı, A. Osherov, N.G. Park, M.O. Reese, F. De Rossi, M. Saliba, U. S. Schubert, H.J. Snaith, S.D. Stranks, W. Tress, P.A. Troshin, V. Turkovic, S. Veenstra, I. Visoly-Fisher, A. Walsh, T. Watson, H. Xie, R. Yıldırım, S. M. Zakeeruddin, K. Zhu, M. Lira-Cantu, Consensus statement for stability assessment and reporting for perovskite photovoltaics based on ISOS procedures, Nat. Energy 5 (2020) 35–49, https://doi.org/10.1038/s41560-019-0529-5.
[26] T. Tayagaki, H. Kobayashi, K. Yamamoto, T.N. Murakami, M. Yoshita, Ultraviolet-light–dark cycle analysis of degradation in perovskite solar cells, Sol. Energy Mater. Sol. Cells 263 (2023) 112583, https://doi.org/10.1016/j.solmat.2023.112583.
[27] X. Zhao, T. Liu, Q.C. Burlingame, T. Liu, R. Holley, G. Cheng, N. Yao, F. Gao, Y. L. Loo, Accelerated aging of all-inorganic, interface-stabilized perovskite solar cells, Science 377 (2022) 307–310, https://doi.org/10.1126/science.abn5679.
[28] T.J. Silverman, M.G. Deceglie, I.R. Repins, T. Zhu, Z. Song, M.J. Heben, Y. Yan, C. Fei, J. Huang, L.T. Schelhas, Daily performance changes in metal halide perovskite PV modules, IEEE J. Photovoltaics 13 (2023) 740–742, https://doi.org/10.1109/JPHOTOV.2023.3289576.
[29] W. Song, T. Aernouts, Novel test scenarios needed to validate outdoor stability of perovskite solar cells, JPhys Energy 2 (2020) 021003, https://doi.org/10.1088/2515-7655/ab6008.
[30] J.H. Wohlgemuth, Development of accelerated stress tests, in: Photovolt. Modul. Reliab., John Wiley & Sons Ltd., Hoboken, 2020, pp. 55–65, https://doi.org/10.1002/9781119459019.ch3.
[31] R. Cheacharoen, N. Rolston, D. Harwood, K.A. Bush, R.H. Dauskardt, M. D. McGehee, Design and understanding of encapsulated perovskite solar cells to withstand temperature cycling, Energy Environ. Sci. 11 (2018) 144–150, https://doi.org/10.1039/c7ee02564e.
[32] A.F. Akbulatov, L.A. Frolova, N.N. Dremova, I. Zhidkov, V.M. Martynenko, S. A. Tsarev, S.Y. Luchkin, E.Z. Kurmaev, S.M. Aldoshin, K.J. Stevenson, P.A. Troshin, Light or heat: what is killing lead halide perovskites under solar cell operation conditions? J. Phys. Chem. Lett. 11 (2020) 333–339, https://doi.org/10.1021/acs.jpclett.9b03308.
[33] M.V. Khenkin, K.M. Anoop, I. Visoly-Fisher, S. Kolusheva, Y. Galagan, F. Di Giacomo, O. Vukovic, B. Ramesh Patil, G. Sherafatipour, V. Turkovic, H.-G. Rubahn, M. Madsen, A.V. Mazanik, E.A. Katz, Dynamics of photoinduced degradation of perovskite photovoltaics: from reversible to irreversible processes, ACS Appl. Energy Mater. 1 (2018) 799–806, https://doi.org/10.1021/acsaem.7b00256.
[34] H.-S. Duan, H. Zhou, Q. Chen, P. Sun, S. Luo, T.-B. Song, B. Bob, Y. Yang, The identification and characterization of defect states in hybrid organic–inorganic perovskite photovoltaics, Phys. Chem. Chem. Phys. 17 (2015) 112–116, https://doi.org/10.1039/c4cp04479g.
[35] A. Dualeh, T. Moehl, M.K. Nazeeruddin, M. Grätzel, Temperature dependence of transport properties of spiro-MeOTAD as a hole transport material in solid-state dye-sensitized solar cells, ACS Nano 7 (2013) 2292–2301, https://doi.org/10.1021/nn4005473.
[36] C.R. Osterwald, T.J. McMahon, History of accelerated and qualification testing of terrestrial photovoltaic modules: a literature review, Prog. Photovoltaics Res. Appl. 17 (2009) 11–33, https://doi.org/10.1002/pip.
[37] D.C. Jordan, N. Haegel, T.M. Barnes, Photovoltaics module reliability for the terawatt age, Prog. Energy. 4 (2022) 022002, https://doi.org/10.1088/2516-1083/ac6111.
[38] International Electrotechnical Commission, IEC 61215-2:2021 Terrestrial Photovoltaic (PV) Modules - Design Qualification and Type Approval - Part 2: Test Procedures, 2021.
[39] B. Hallam, A. Ciesla, M. Abbott, Progress in the understanding of light- and elevated temperature-induced degradation in silicon solar cells : a review, Prog. Photovoltaics Res. Appl. 29 (2021) 1180–1201, https://doi.org/10.1002/pip.3362.
[40] I.L. Repins, D.C. Jordan, M. Woodhouse, M. Theristis, J.S. Stein, H.P. Seigneur, D. J. Colvin, J.F. Karas, A.N. McPherson, C. Deline, Long-term impact of light- and elevated temperature-induced degradation on photovoltaic arrays, MRS Bull. 48 (2023) 589–601, https://doi.org/10.1557/s43577-022-00438-8.
[41] J. Karas, I. Repins, F. Jiang, D. Zhang, K.A. Berger, B. Kubicek, J. Jaubert, A. B. Cueli, B. Jaeckel, M. Pander, E. Fokuhl, T. Sample, M.B. Koentopp, F. Kersten, J. C. Birinchi, G. Bellenda, Results from an international interlaboratory study on light-and elevated temperature-induced degradation in solar modules, Prog. Photovoltaics Res. Appl. 30 (2022) 1255–1269, https://doi.org/10.1002/pip.3573.
[42] M. Wang, H. Wang, W. Li, X. Hu, K. Sun, Z. Zang, Defect passivation using ultrathin PTAA layers for efficient and stable perovskite solar cells with a high fill factor and eliminated hysteresis, J. Mater. Chem. A 7 (2019) 26421–26428, https://doi.org/10.1039/c9ta08314f.
[43] R. Azmi, E. Ugur, A. Seitkhan, F. Aljamaan, A.S. Subbiah, J. Liu, G.T. Harrison, M. I. Nugraha, M.K. Eswaran, M. Babics, Y. Chen, F. Xu, T.G. Allen, A. Rehman, C. Wang, T.D. Anthopoulos, U. Schwingenschlögl, M. De Bastiani, E. Aydin, S. De Wolf, Damp heat–stable perovskite solar cells with tailored-dimensionality 2D/3D heterojunctions, Science 376 (2022) 73–77, https://doi.org/10.1126/science.abm5784.
[44] W.H. Zhang, L. Chen, Z.P. Zou, Z.A. Nan, J.L. Shi, Q.P. Luo, Y. Hui, K.X. Li, Y. J. Wang, J.Z. Zhou, J.W. Yan, B.W. Mao, Defect passivation by a multifunctional phosphate additive toward improvements of efficiency and stability of perovskite solar cells, ACS Appl. Mater. Interfaces 14 (2022) 31911–31919, https://doi.org/10.1021/acsami.2c05956.
[45] H. Li, C. Zhang, C. Gong, D. Zhang, H. Zhang, Q. Zhuang, X. Yu, S. Gong, X. Chen, J. Yang, X. Li, R. Li, J. Li, J. Zhou, H. Yang, Q. Lin, J. Chu, M. Grätzel, J. Chen, Z. Zang, 2D/3D heterojunction engineering at the buried interface towards high-performance inverted methylammonium-free perovskite solar cells, Nat. Energy 8 (2023) 946–955, https://doi.org/10.1038/s41560-023-01295-8.
[46] C. Zhang, H. Li, C. Gong, Q. Zhuang, J. Chen, Z. Zang, Crystallization manipulation and holistic defect passivation toward stable and efficient inverted perovskite solar cells, Energy Environ. Sci. 16 (2023) 3825–3836, https://doi.org/10.1039/d3ee00413a.
[47] C. Li, X. Wang, E. Bi, F. Jiang, S.M. Park, Y. Li, L. Chen, Z. Wang, L. Zeng, H. Chen, Y. Liu, C.R. Grice, A. Abudulimu, J. Chung, Y. Xian, T. Zhu, H. Lai, B. Chen, R. J. Ellingson, F. Fu, D.S. Ginger, Z. Song, E.H. Sargent, Y. Yan, Rational design of Lewis base molecules for stable and efficient inverted perovskite solar cells, Science 379 (2023) 690–694, https://doi.org/10.1126/science.ade3970.
[48] S. Mariotti, E. Köhnen, F. Scheler, K. Sveinbjörnsson, L. Zimmermann, M. Piot, F. Yang, B. Li, J. Warby, A. Musiienko, D. Menzel, F. Lang, S. Keßler, I. Levine, D. Mantione, A. Al-Ashouri, M.S. Härtel, K. Xu, A. Cruz, J. Kurpiers, P. Wagner, H. Köbler, J. Li, A. Magomedov, D. Mecerreyes, E. Unger, A. Abate, M. Stolterfoht, B. Stannowski, R. Schlatmann, L. Korte, S. Albrecht, Interface engineering for high-performance, triple-halide perovskite-silicon tandem solar cells, Science 381 (2023) 63–69, https://doi.org/10.1126/science.adf5872.